




Structural rearrangements and fragmentation pathways induced by a low-energy electron attachment to ethyl acetate

Anirban Paul ¹, Ian Carmichael ², Dhananjay Nandi,^{1,3} Sylwia Ptasinska,^{2,4,*} and Dipayan Chakraborty ^{2,†}

¹Indian Institute of Science Education and Research Kolkata, Mohanpur 741246, India

²Radiation Laboratory, University of Notre Dame, Notre Dame, Indiana 46556, USA

³Center for Atomic, Molecular and Optical Sciences and Technologies, Joint initiative of IIT Tirupati and IISER Tirupati, Yerpedu 517619, Andhra Pradesh, India

⁴Department of Physics and Astronomy, University of Notre Dame, Notre Dame, Indiana 46556, USA



(Received 4 January 2024; accepted 28 March 2024; published 18 April 2024)

The phenomenon of dissociative electron attachment to ethyl acetate is investigated within the 1 to 13 eV energy region. The recorded yields of various fragment anions within the above-mentioned energy range reveal a diverse array of products with six different mass numbers. Examples include $(M - H)^-$, CH_3^- , $C_2H_5O^-$, CH_3CO^- , CH_2CHO^- , and CH_3COO^- , formed through the fracture of single bonds. Interestingly, the generation of other fragments, such as $HCCO^-$, suggests a more intricate structural rearrangement of the nuclei, adding a layer of complexity to the observed dissociation dynamics.

DOI: [10.1103/PhysRevA.109.042818](https://doi.org/10.1103/PhysRevA.109.042818)

I. INTRODUCTION

Dissociative electron attachment (DEA) is the dominant process leading to the dissociation of molecules in low-energy electron collisions that have been experimentally observed. It is a two-step resonant process; in the first step, the incoming electron resonantly attaches to the molecule, producing a temporary negative ion (TNI). In the subsequent step, the TNI dissociates, producing an anionic fragment along with one or more neutral fragments [1–8]. This process has diverse involvement in different fields, from atmospheric chemistry [9] to the damage to living cells during radiation therapy [10].

Ethyl acetate is among the simplest esters, a class of compounds derived from acids where the hydrogen atom of at least one acidic hydroxyl group ($-OH$) is replaced by an organyl group ($-R$). Esters are ubiquitous in nature and are extensively used in various industries. The pleasant aroma of many fruits, for instance, can be attributed to the presence of esters. Fats, on the other hand, are primarily triesters derived from glycerol and fatty acids, with glycerides representing fatty acid esters of glycerol and lactones being cyclic carboxylic esters. Ethyl acetate is a colorless liquid with a sweet, fruity odor that is generally well received. It serves as a widely used solvent, particularly in the production of paints, varnishes, lacquers, cleaning mixtures, and perfumes [11–13]. Additionally, it is employed as a solvent in processes such as decaffeinating coffee beans and in column and thin-layer chromatography in laboratory settings [14,15]. Furthermore, it serves as an asphyxiant for insect collection for study purposes. Industrially, ethyl acetate is primarily synthesized through the classic

Fischer esterification reaction involving ethanol and acetic acid [16,17].

Due to its widespread usage in industry, ethyl acetate has been detected in the atmosphere, making it a potential source of CO_2 [18]. Therefore, it is important to study its decomposition in the atmosphere through interaction with low-energy electrons. Despite its extensive use in research and industry, there has been no study on DEA to ethyl acetate to date [11–15]. Additionally, only a few reports exist on DEA to esters [19–21]. Feketeová *et al.* [20] investigated the DEA dynamics of methyl acetate by measuring the yields of various fragment anions as a function of incident electron energies. They observed that these fragment anions were produced from one *shape resonance* at approximately 2.5 eV, along with several *Feshbach resonances* in the range of 6–12 eV electron energy. Pariat and Allan explored the DEA dynamics of methyl acetate by measuring the yields of different fragment anions [19]. They identified one shape resonance near 3 eV and three higher-energy Feshbach resonances in the 6–12 eV range. Several anionic fragments were observed, including CH_3^- , CH_3CO^- , CH_3O^- , $HCCO^-$, CHO^- , CH_2COO^- and $CH_2COOCH_3^-$ ions. They proposed a mechanism for the production of $HCCO^-$ involving the rapid stabilization of the primary resonance by the loss of an H atom, followed by a slower process of proton transfer. The $HCCO^-$ anions produced due to low-energy electron collisions can act as a source of CO_2 . These anions react with molecular oxygen, producing CO_2 [19].

The aim of this study is to understand the detailed dissociation dynamics by low-energy electron attachment to ethyl acetate. The complete fragmentation process, involving various fragment anions along with their respective dissociation channels, is presented. A quadrupole mass spectrometer was employed to collect ion yields of different fragment anions, and quantum chemical calculations were conducted to

*sptasins@nd.edu

†dchakra2@nd.edu

determine the threshold energies required for the generation of these fragment anions. The investigation indicates a complex structural rearrangement in the negative-ion resonant state is involved in the dissociation process.

II. EXPERIMENTAL AND COMPUTATIONAL METHODS

The experimental setup used to obtain ion-yield curves for negative ions was previously detailed [6]. The experiment was conducted within an ultrahigh-vacuum chamber with a base pressure of 1×10^{-10} mbar, using a Quadrupole Mass Spectrometer (QMS) by Hiden Analytical. In the present study, the system was employed for gas-phase detection of anions. An effusive beam of gas-phase molecules interacted with low-energy electrons generated by the oxide-coated iridium filament within the QMS. The filament emitted electrons through thermionic emission with controlled energy, typically at an intensity of $2.5 \mu\text{A}$. When the low-energy electrons interacted with the molecules, negative fragment ions were produced and collected by a secondary-electron-multiplier (SEM) detector with a selected mass-to-charge ratio m/z . The collection efficiency of the QMS was maximized by varying the focusing voltage while collecting O^- ions from DEA to O_2 at the 6.5 eV resonance. The multiplier voltage of the SEM detector was set in the saturation region accordingly. Energy scans were conducted from 1 to 13 eV, with 0.1 eV increments for each negative fragment generated through the DEA process. These energy scans were executed using the MASSOFT version 7 professional software provided by Hiden. The energy resolution of the electron beam used in the experiment was 0.5 eV. The chamber was baked at 363 K for several days before introducing the sample to reduce signals originating from contamination and the background water that can present in the chamber. The electron energy scale was calibrated by measuring the resonant peak of O^- ion yield resulting from DEA to O_2 at 6.5 eV [22]. Subsequently, the calibration was cross-checked by measuring the resonant peak of O^- ion yield resulting from DEA to CO_2 at 4.3 eV [22]. Energy calibration was performed both before and after the experiment was conducted in order to counter any possible changes during the experiment. The experiments were carried out using 99.5% pure anhydrous ethyl acetate samples from Sigma-Aldrich, which is liquid at room temperature. The sample was introduced from a glass vial and transported to the interaction region through a pipeline connection. The pipeline was linked to an internal capillary within the vacuum chamber that guided the gas-phase sample to the QMS aperture. The sample underwent freeze-pump-thaw cycles several times to eliminate contaminants before it was introduced into the vacuum chamber. The chamber pressure during the experiment was maintained at approximately 1.5×10^{-6} mbar. The experiment was repeated multiple times for each fragment, and the results were consistent in each case.

Quantum chemical calculations were conducted using the GAUSSIAN 16 software [23]. Thermodynamic threshold energies for each dissociation channel were determined using the composite W1 method, [24] employing the Becke three-parameter Lee-Yang-Parr (B3LYP) functional [25] and the flexible correlation-consistent polarized valence triple zeta (cc-pVTZ) basis set [26] for geometry optimizations and basic

TABLE I. Resonant positions of the fragment anions obtained in DEA to ethyl acetate. The peaks observed in the photoabsorption spectra (PES) obtained from Ref. [29] are also added for comparison.

Mass (Da)	Assignment of ions	Peak position (eV)		
		Shape resonance	Feshbach resonance	PES
15	CH_3^-		5.7, 7.3, 8.5, 10.1	5.9, 7.7, 8.8, 9.8
41	HCCO^-	3.3	7.0, 9.7	
43	CH_3CO^-		7.3, 8.2, 10.1	
45	CH_2CHO^-	3.0	7.3, 9.9	
59	CH_3COO^-	3.0	8.9, 10.2	
87	$\text{CH}_2\text{COOCH}_2\text{CH}_3^-$			
	$\text{CH}_3\text{COOCH}_2\text{CH}_2^-$	2.7		
	$\text{CH}_3\text{COOCHCH}_3^-$			

thermochemistry. These calculations were complemented by a series of correlation corrections [27] to ensure high-level accuracy. The threshold energy for a specific dissociation channel of ethyl acetate was determined by calculating the bond dissociation energies involved and the electron affinity of the fragment.

III. RESULTS AND DISCUSSION

A total of six mass fragments at 15, 41, 43, 45, 59, and 87 u have been identified. It is important to note that six mass numbers do not necessarily indicate the presence of six distinct fragment anions. Due to the complexity of the fragmentation process, anions with different molecular structures but with the same mass number are possible. The assignment of these masses to various fragment anions is provided in Table I.

The production of the fragments CH_3^- , CH_3CO^- , $\text{C}_2\text{H}_5\text{O}^-$, and CH_3COO^- and the H-loss anions $[(M - \text{H})^-]$ can be attributed to single-bond breaking. In contrast, the generation of HCCO^- and CH_2CHO^- involves multiple-bond breaking and/or complex structural rearrangement in the negative-ion resonant state [28]. The absence of C_2H_5^- ions can be explained by the negative electron affinity of C_2H_5 . For reference, the electron affinities of the neutral counterparts of several fragment anions are provided in Table II.

In the following sections, we will first examine the ions produced through single-bond breaking or direct dissociation. Subsequently, we will delve into the production of ions, which implies complex structural rearrangements. We obtained the negative-ion yields of different fragment anions produced from DEA to ethyl acetate as a function of incident electron energy ranging from 1 to 13 eV, and the resulting fragment anions, along with their respective assignments and resonance positions, are provided in Table I.

A. Production of H-loss anions $[(M - \text{H})^-]$, $M = 87$

The yield of $(M - \text{H})^-$ ions as a function of electron energy during DEA to ethyl acetate is depicted in Fig. 1. This ion yield exhibits a prominent peak centered around 2.7 eV that can be attributed to resonance with a π^* character. A previous

TABLE II. Electron affinities (EAs) of selected neutrals and the corresponding bond dissociation energies (BDEs).

Species	EA (eV)
CH ₃	0.029
C ₂ H ₅	-0.236
CH ₃ CO	0.403
CH ₂ CHO	1.837
HCCO	2.353
C ₂ H ₅ O	1.678
CH ₃ COO	3.328
CH ₃ COOCH ₂	0.478
CH ₂ COOC ₂ H ₅	1.692
CH ₃ COOCHCH ₃	0.355
Bond	BDE (eV)
CH ₃ -COOC ₂ H ₅	4.04
CH ₃ CO-OC ₂ H ₅	4.30
CH ₃ COO-C ₂ H ₅	3.89
CH ₃ COOCH ₂ -CH ₃	3.84
H-CH ₂ COOC ₂ H ₅	4.24
CH ₃ COOCH-HCH ₃	4.18
CH ₃ COOCH ₂ CH ₂ -H	4.39

photoabsorption study on ethyl acetate indicated that the lowest unoccupied molecular orbital predominantly exhibits π^* antibonding character and is localized on the C=O bond [29]. During the attachment, the incoming electron can be captured by the unoccupied π^* (C=O) orbital, leading to the formation of the TNI state, which subsequently dissociates, producing various fragment anions. In the current investigation, the observed resonance at 2.7 eV is attributed to this π^* shape resonance. In a previous study of DEA to methyl acetate, a similar resonance in this energy range was also identified and attributed to a π^* resonance [19]. In the context of the TNI state, three distinct dissociation channels leading to fragment anions with the same mass number but different molecular

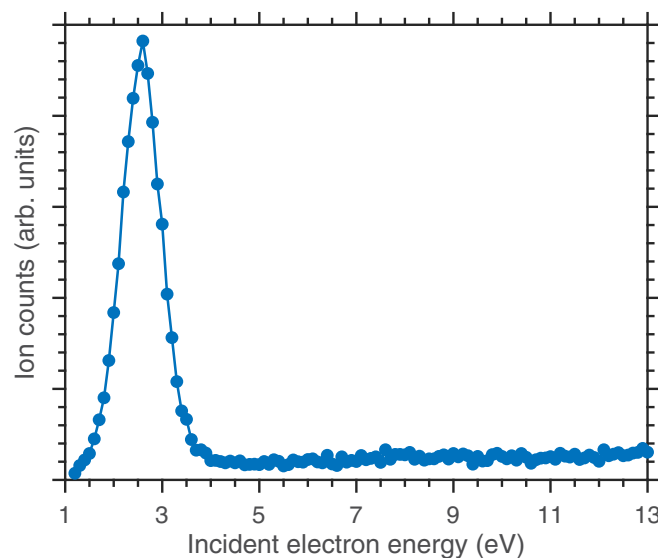
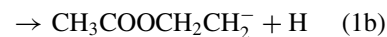


FIG. 1. Ion-yield curve of $(M - H)^-$ ions produced due to DEA to ethyl acetate in the energy range of 1–13 eV. A single resonant peak at 2.7 eV is observed.

structures are possible, depending on the site of the H loss [30,31]. These three H-loss anions are $\text{CH}_2\text{COOCH}_2\text{CH}_3^-$, $\text{CH}_3\text{COOCH}_2\text{CH}_2^-$, and $\text{CH}_3\text{COOCHCH}_3^-$. The first one is formed by breaking a C–H bond from the methyl group. In contrast, the second and third ones are generated by breaking a C–H bond within the CH_3 and CH_2 groups, respectively, of the ethyl moiety. These ions are exclusively produced through the cleavage of a single C–H bond. The possible dissociation channels responsible for producing these H-loss anions can be represented as follows:



The present theoretical investigation indicates that $\text{CH}_3\text{COOCH}_2\text{CH}_2^-$ ions in channel (1b) are inherently unstable and undergo spontaneous dissociation, yielding a CH_3COO^- ion along with a neutral conjugate of CH_2CH_2 [channel (5b)]. Consequently, channel (1b) can be disregarded for the generation of $(M - H)^-$ ions. The calculated threshold energies for channels (1a) and (1c) are 2.55 and 3.83 eV, respectively.

As we investigated the H-loss channels, our anticipation was to observe the H^- ions by breaking the same bond with their conjugate neutral counterparts within this energy range. However, our current experimental limitations prevent us from verifying this expectation. The QMS spectrometer used in this experiment lacks the capability to detect H^- ions.

B. Production of CH_3^- ions ($M = 15$)

Figure 2 illustrates the ion-yield curve of CH_3^- ions resulting from DEA to ethyl acetate. A broad range of overlapping resonances, spanning from 6 to 12 eV, is observed, accompanied by a hump near 5.7 eV. To locate the correct positions of these overlapping resonances, we opted to fit the CH_3^- ion yield using multiple Gaussian functions, as depicted in Fig. 2. The fitted ion-yield curve indicates the likely presence of three closely lying resonant bands in the 6 to 12 eV energy range, peaking at 7.3, 8.5, and 10.1 eV, respectively. However, due to the limited energy resolution (0.5 eV) of the electron beam and the finite width of the resonances, it is not feasible to distinctly separate them in the present study.

These different resonances were compared to the vacuum ultraviolet (VUV) photoabsorption study [29]. That study suggested the existence of an absorption band in the vicinity of 5.9 eV, attributed to the highest occupied molecular orbital to $\pi^*(\text{C}=\text{O})$ transition. Additionally, the authors suggested the occurrence of multiple Rydberg transitions spanning the 6.5–10 eV range, as shown in Fig. 2. These Rydberg states are proposed to act as parent states for the DEA resonances observed in the present investigation. Through comparison with the earlier report, the four DEA resonances identified within the 5 to 12 eV energy range are likely to be *core-excited Feshbach* resonances [29]. The first band in the photoabsorption spectra, which peaks at approximately 5.9 eV, may serve as the parent state for the weak resonance detected at 5.7 eV. Likewise, the second band, reaching its peak at about 7.7 eV, could be the parent state for the sharp resonance identified at

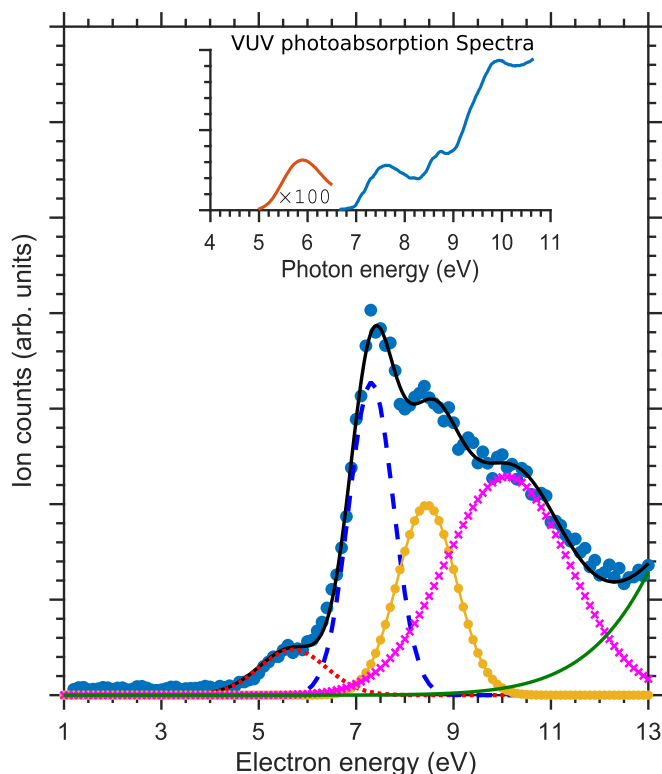
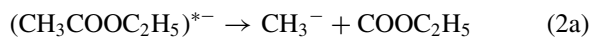


FIG. 2. The VUV photoabsorption spectrum of ethyl acetate was extracted from a previous report [29]. This spectrum reveals the presence of four absorption bands within the 5–10 eV energy region. The ion yield of CH_3^- ions produced due to DEA to ethyl acetate in the energy range of 1–13 eV is also presented at the bottom. The blue dots represent the experimental data points, and the black solid curve indicates the cumulative fitted curve with four Gaussian functions attributed to four resonant bands (illustrated in red, blue, yellow, and pink). One exponential function is also shown to incorporate the contribution of the IP dissociation process (solid green curve). The fitting suggests that the structure present in the 5–12 eV range is a combination of four resonant states with energies at 5.7, 7.3, 8.5, and 10.1 eV.

7.3 eV. Similarly, the remaining two bands, with peaks around 8.8 and 9.8 eV, may correspond to the parent states for resonances at 8.5 and 10.1 eV, respectively. A comparison between the VUV photoabsorption spectrum [29] and the CH_3^- ion yield is depicted in Fig. 2.

The CH_3^- formation could be through a simple two-body dissociation process either from the methyl site or from the ethyl moiety, as shown by the reaction channels

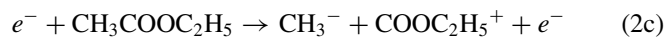


In channel (2a), CH_3^- ions are produced from the $-\text{CH}_3$ site, while in channel (2b), CH_3^- ions are produced from the $-\text{C}_2\text{H}_5$ moiety. The theoretically calculated threshold values for these channels are 4.01 and 3.81 eV, respectively. However, it is intriguing to explore whether three-body or even higher-order dissociation of the TNI is possible. By examining the resonance positions, we can suggest that the 5.7 eV resonance primarily involves two-body

dissociation, whereas the 7.3, 8.5, and 10.1 eV resonances may either undergo two-body dissociation with significantly high rovibrational excited fragments or involve three-body or higher-order dissociations. To offer a definitive answer, measuring the kinetic energy of the CH_3^- fragments would be necessary, which goes beyond the scope of the present study.

It is worth mentioning that if the production of CH_3^- occurs due to the breaking of the $\text{H}_3\text{C}-\text{COOC}_2\text{H}_5$ bond, there should also be a possibility of producing $\text{COOC}_2\text{H}_5^-$ ions. Conversely, if CH_3^- ions are produced due to the breaking of the $\text{CH}_3\text{COOCH}_2-\text{CH}_3$ bond, there should be a chance of producing $\text{CH}_3\text{COOCH}_2^-$ ions. Both $\text{COOC}_2\text{H}_5^-$ and $\text{CH}_3\text{COOCH}_2^-$ have a mass of 73, which is absent from our mass spectra. Our theoretical calculations suggest that the former ion spontaneously dissociates to produce one $\text{C}_2\text{H}_5\text{O}^-$ ion and one CO molecule [channel (3b)]. However, $\text{CH}_3\text{COOCH}_2^-$ is a stable species with a positive electron affinity. The computed threshold energy for the production of this anion is 3.36 eV. The absence of $\text{CH}_3\text{COOCH}_2^-$ in the present results may be due to either the $\text{CH}_3\text{COOCH}_2-\text{CH}_3$ bond not breaking to produce CH_3^- ions or, if the $\text{CH}_3\text{COOCH}_2-\text{CH}_3$ bond did break, $\text{CH}_3\text{COOCH}_2^-$ not being produced. However, electron-affinity calculations suggest that the electron affinity of CH_3 (0.029 eV) is lower than that of $\text{CH}_3\text{COOCH}_2$ (0.478 eV). This implies that the probability of producing $\text{CH}_3\text{COOCH}_2^-$ should be higher than that of CH_3^- . This observation likely indicates the nondissociative nature of the $\text{CH}_3\text{COOCH}_2-\text{CH}_3$ bond upon electron attachment to ethyl acetate. Hence, the observed CH_3^- ions are coming from the $\text{H}_3\text{C}-\text{COOC}_2\text{H}_5$ dissociation [channel (2a)]. In this context, we aim to highlight the observations made regarding DEA to methyl acetate molecules [19]. Methyl acetate belongs to the same ester group for which Pariat *et al.* [19] experimentally demonstrated the nondissociative nature of the $\text{H}_3\text{CCOO}-\text{CH}_3$ bond. Their findings indicate that the formation of CH_3^- is favored through dissociation from the $\text{H}_3\text{C}-\text{COOCH}_3$ site [19].

A continuous increase in ion counts with increasing incident electron energy is observed above 11 eV. This behavior is due to the involvement of the CH_3^- ions formed due to the ion-pair (IP) dissociation [32,33]. For other fragment anions, the threshold of the IP states lies above 14 eV and hence is absent in the measured ion yield. However, that is not the case for the CH_3^- ions, where the calculated IP threshold lies around 11.1 eV. The CH_3^- ion-yield feature at higher energies agrees with our theoretically calculated IP threshold. It is worth investigating why the IP states near 11.1 eV dissociate by producing only the CH_3^- ions. Two possible channels producing CH_3^- ions through the IP dissociation are



The theoretically computed threshold values of these two channels are 11.13 and 11.15 eV, respectively. The overlap between the DEA and the IP dissociation is observed from the CH_3^- ion yield. In order to include the contribution from the IP dissociation in the ion yield, we fitted it with an exponential function (along with the Gaussian functions) as shown in Fig. 2.

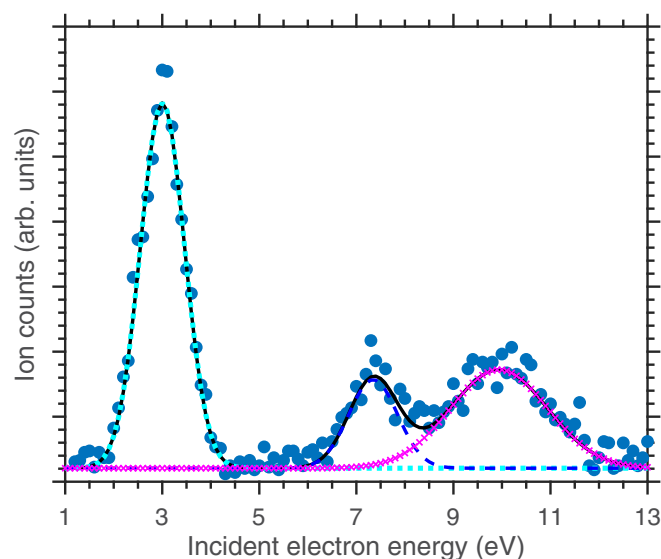


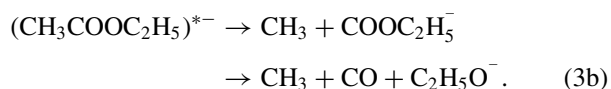
FIG. 3. The ion yield of $\text{C}_2\text{H}_5\text{O}^-$ ions produced due to DEA to ethyl acetate in the energy range of 1 to 13 eV. The blue dots represent the experimental data points, and the black solid line represents the cumulative fit of the ion yield with three Gaussian functions (illustrated in sky blue, dark blue, and pink). The fitting suggests that the structure present in the 3.0 eV region is due to the contribution of a shape resonance, whereas the 6–12 eV region is a combination of two core-excited Feshbach resonances peaking at 7.3 and 9.9 eV.

C. Production of $\text{C}_2\text{H}_5\text{O}^-$ ions ($M = 45$)

Figure 3 illustrates the ion yield of $\text{C}_2\text{H}_5\text{O}^-$ resulting from DEA to ethyl acetate. A distinct and intense peak is observed at 3 eV, accompanied by two broad resonances peaking at 7.3 and 9.9 eV. Due to the broad nature of these resonant states, the contribution of other resonances with a lower cross section cannot be ruled out in this energy region. The mechanism for the formation of $\text{C}_2\text{H}_5\text{O}^-$ ions during the DEA process is through the dissociation of the $\text{CH}_3\text{OC}-\text{OC}_2\text{H}_5$ bond. This simple two-body dissociation can be represented as follows:



The calculated threshold energy for this channel is 2.62 eV, making it the only possible candidate for the observed 2.9 eV shape resonance. The experimentally obtained appearance energy aligns well with the computed threshold energy, considering the resolution of the electron beam used in the experiment. Regarding the Feshbach resonances within the 6 to 12 eV region, three-body or even higher-order dissociation might be involved. One such possible sequential dissociation channel is



The calculated threshold energy for this channel is 3.04 eV, making it a potential candidate for the Feshbach resonances. This proposed dissociation channel (3b) could be either a concerted three-body dissociation or a sequential dissociation. The dissociation of the $\text{H}_3\text{C}-\text{COOC}_2\text{H}_5$ bond produces CH_3^- ions with a neutral COOC_2H_5 conjugate. This introduces the

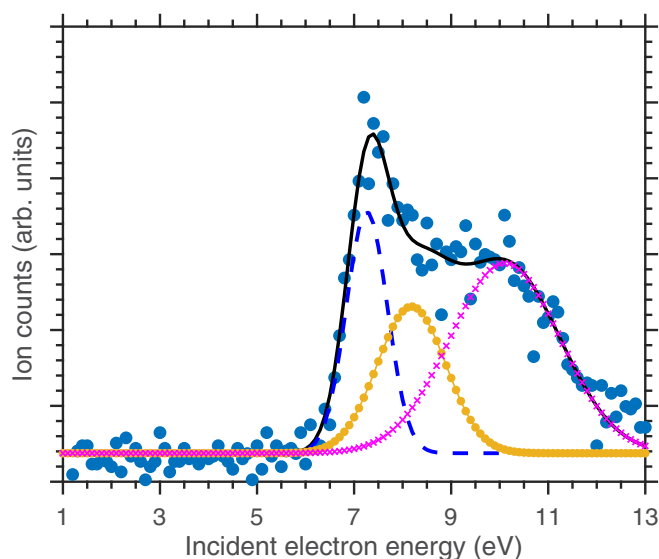


FIG. 4. The ion yield of CH_3CO^- ions produced due to DEA to ethyl acetate in the energy range of 1 to 13 eV. The blue dots represent the experimental data points, and the black solid line represents the cumulative fit of the ion yield with three Gaussian functions (illustrated in blue, yellow, and pink). The fitting suggests that the structure present in the 6–12 eV region is a combination of three core-excited Feshbach resonances peaking at 7.3, 8.2, and 10.1 eV.

possibility of observing $\text{COOC}_2\text{H}_5^-$ ions in the DEA process. However, we did not detect the presence of $\text{COOC}_2\text{H}_5^-$ in the measurements. One of the reasons for this could be its unstable nature or its short lifetime. It is possible that $\text{COOC}_2\text{H}_5^-$ ions are, indeed, formed in the DEA process but, due to their unstable nature, they spontaneously dissociate to produce CO and $\text{C}_2\text{H}_5\text{O}^-$ ions. The presence of Feshbach resonances within the 6 to 12 eV region for the CH_3^- ions reinforces this conclusion. This observation suggests that a sequential dissociation of the TNI may be involved.

D. Production of CH_3CO^- and CH_2CHO^- ions ($M = 43$)

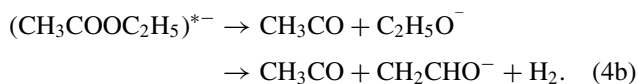
Figure 4 depicts the ion yield of mass 43 produced due to low-energy electron attachment to ethyl acetate. The presence of Feshbach resonances within the 6 to 12 eV region is detected. However, no contribution from the shape resonance is observed for fragments with this mass. Two anions, CH_3CO^- and CH_2CHO^- , can be generated through the dissociation of ethyl acetate with a mass of 43. The mechanism producing CH_3CO^- is through a two-body dissociation by breaking the $\text{CH}_3\text{OC}-\text{OC}_2\text{H}_5$ bond, resulting in CH_3CO^- ions with $\text{C}_2\text{H}_5\text{O}$ as the neutral. The dissociation pathway for this fragment is as follows:



This is essentially the conjugate dissociation process of $\text{C}_2\text{H}_5\text{O}^-$ formation [channel (3a)], in which we observed a strong signal due to the contribution from the shape resonance within the 1 to 4 eV energy region (Fig. 3). However, no ion signal within the 1 to 4 eV region is observed in the CH_3CO^- channel. The higher threshold energy of this dissociation channel is the reason behind the exclusion of the shape

resonance, as we found the computed threshold energy to be around 3.9 eV.

On the other hand, the production of CH_2CHO^- ions requires many-body dissociation and rearrangements in the TNI. This dissociation begins with the production of $\text{C}_2\text{H}_5\text{O}^-$, which simultaneously or sequentially dissociates, producing CH_2CHO^- and H_2 . The presence of $\text{C}_2\text{H}_5\text{O}^-$ ions within the 6 to 12 eV Feshbach resonance region (Fig. 3) makes this a candidate dissociation pathway. The only conceivable reason to exclude this channel would be the stability of $\text{C}_2\text{H}_5\text{O}^-$ ions. This process can be represented as



The computed threshold energy of this channel is 2.74, which is in agreement with the present experimental results. Despite the observed shape resonance character of $\text{C}_2\text{H}_5\text{O}^-$ (Fig. 3), no CH_2CHO^- was observed in this energy region. The likely explanation is the presence of a potential barrier hindering the direct dissociation of $\text{C}_2\text{H}_5\text{O}^-$ ions. For the higher resonances, the substantial difference between the threshold energy and the incident electron energy yields more excess available energy for the dissociation process. This leads to the formation of $\text{C}_2\text{H}_5\text{O}^-$ fragments in significantly elevated energy states. Consequently, the dissociation of $\text{C}_2\text{H}_5\text{O}^-$ ions into CH_2CHO^- ions and other fragments becomes possible.

E. Production of CH_3COO^- ions ($M = 59$)

The yield of CH_3COO^- ions as a function of the electron energy from DEA to ethyl acetate is depicted in Fig. 5. Two broad resonances peaking at 3 and 9 eV are observed. The higher-energy resonant feature ranges from 6 to 12 eV, indicating the presence of similar Feshbach resonances observed for other fragments. The mechanism for CH_3COO^- ion production is through a two-body dissociation channel by breaking the $\text{CH}_3\text{COO}-\text{C}_2\text{H}_5$ bond. The dissociation channel can be represented as follows:



The computed threshold energy for this dissociation channel is 0.57 eV, making this channel plausible for the 3 eV resonance. For the higher resonances, three-body or higher-order dissociation may be involved. It is worth mentioning that since the production of CH_3COO^- occurs due to the breaking of the $\text{CH}_3\text{COO}-\text{C}_2\text{H}_5$ bond, there should also be a possibility of the production of C_2H_5^- ions. However, the present measurement confirms no C_2H_5^- forms due to the low-energy electron collision. Our theoretical calculation suggests that C_2H_5 has negative electron affinity, and thus, the production of C_2H_5^- is not possible.

Another possible dissociation channel for the formation of the CH_3COO^- ions is through a sequential dissociation of the TNI. As mentioned in Sec. III A, $\text{CH}_3\text{COOCH}_2\text{CH}_2^-$ [channel (1b)] ion is extremely unstable and simultaneously dissociates to produce a CH_3COO^- ion with a CH_2CH_2 neutral conjugate. The dissociation mechanism can be represented in the

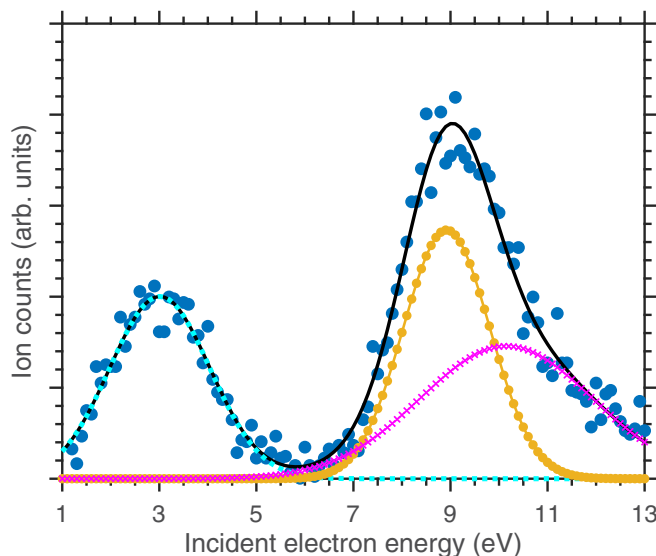
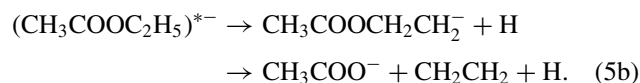


FIG. 5. The ion yield of CH_3COO^- ions produced due to DEA to ethyl acetate in the energy range of 1 to 13 eV. The blue dots represent the experimental data points, and the black solid line represents the cumulative fit of the ion yield with three Gaussian functions (illustrated in sky blue, yellow, and pink). The fitting suggests that the structure present in the 3 eV region is due to the contribution of a shape resonance, whereas the 6–12 eV region is a combination of two core-excited Feshbach resonances peaking at 8.9 and 10.2 eV.

following way:



The computed threshold energy for this dissociation channel is 2.31 eV, making it a candidate for both lower- and higher-energy resonances.

F. Production of HCCO^- ions ($M = 41$)

Figure 6 illustrates the ion-yield curve of mass 41 resulting from low-energy electron attachment to ethyl acetate. One small peak near 3.3 eV and a broad peak near 9.7 eV are observed, along with a small hump near 7 eV. To clearly locate these resonances, we opted to fit the ion yield with three Gaussian functions, as shown in Fig. 6. Mass 41 can be attributed to the formation of HCCO^- ions. This is likely the only fragment that cannot be produced through a single-bond dissociation process; instead, complex structural rearrangements in the TNI are essential. Various dissociation channels producing HCCO^- ions are listed in Table III. Complex structural changes are involved in all these channels. To elucidate this process, we can refer to Fig. 7. The formation of HCCO^- fragments can proceed through C–O dissociation either near the keto site or near the ethyl site. We discuss the processes below.

1. C–O dissociation near the keto site

In this dissociation channel, molecular H_2 forms as a by-product. The dissociation can occur through a concerted three-body process involving structural rearrangements in the

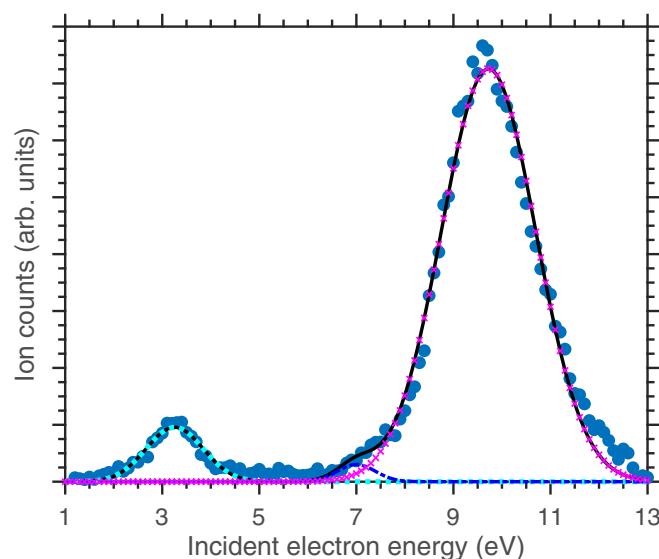


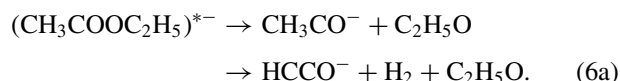
FIG. 6. The ion yield of HCCO^- ions produced due to DEA to ethyl acetate in the energy range of 1 to 13 eV. The blue dots represent the experimental data points, and the black solid line represents the cumulative fit of the ion yield with three Gaussian functions (illustrated in sky blue, dark blue, and pink). The fitting suggests that the structure present in the 3.3 eV region is due to the contribution of a shape resonance, whereas the 6–12 eV region is a combination of two core-excited Feshbach resonances peaking at 7 and 9.7 eV.

TNI. One C–O bond dissociates, two C–H bonds dissociate from the $\text{CH}_3\text{C}=\text{O}$ site, and a H–H bond forms during this process. The final dissociated products of this channel are shown in channel (6a). Alternatively, HCCO^- can form through a sequential dissociation process. In the first step, the C–O bond dissociates, leading to the formation of CH_3CO^- and the neutral conjugate $\text{C}_2\text{H}_5\text{O}$ [as shown in channel (4a)].

TABLE III. Dissociation channels producing different fragment anions and their computed threshold values.

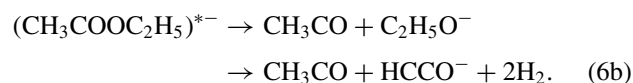
Channel	Dissociative products	Threshold energy (eV)
(1a)	$\text{CH}_3\text{COOCH}_2\text{CH}_2^- + \text{H}$	2.55
(1c)	$\text{CH}_3\text{COOCHCH}_3^- + \text{H}$	3.83
(2a)	$\text{CH}_3^- + \text{COOC}_2\text{H}_5$	4.01
(2b)	$\text{CH}_3^- + \text{CH}_3\text{COOCH}_2$	3.81
(2c)	$\text{CH}_3^- + \text{COOC}_2\text{H}_5^+$	11.13
(2d)	$\text{CH}_3^- + \text{CH}_3\text{COOCH}_2^+$	11.15
(3a)	$\text{CH}_2\text{CH}_3\text{O}^- + \text{CH}_3\text{CO}$	2.62
(3b)	$\text{CH}_2\text{CH}_3\text{O}^- + \text{CH}_3 + \text{CO}$	3.04
(4a)	$\text{CH}_3\text{CO}^- + \text{C}_2\text{H}_5\text{O}$	3.90
(4b)	$\text{CH}_3\text{CO} + \text{CH}_2\text{CHO}^- + \text{H}_2$	2.74
(5a)	$\text{CH}_3\text{COO}^- + \text{C}_2\text{H}_5$	0.57
(5b)	$\text{CH}_3\text{COO}^- + \text{CH}_2\text{CH}_2 + \text{H}$	2.31
(6a)	$\text{HCCO}^- + \text{C}_2\text{H}_5\text{O} + \text{H}_2$	3.85
(6b)	$\text{HCCO}^- + \text{CH}_3\text{CO} + 2\text{H}_2$	3.85
(6c)	$\text{HCCO}^- + \text{C}_2\text{H}_5 + \text{H}_2\text{O}$	2.73

In the second step, CH_3CO^- further dissociates to form HCCO^- and H_2 . The process can be represented as follows:



The computed threshold for the concerted three-body dissociation processes is 3.85 eV, indicating that the 3.3 eV shape resonance cannot proceed through this channel. Alternatively, for the intermediate step, the computed threshold energy is 3.90 eV [channel (4a)]. As a result, the formation of HCCO^- from the 3.3 eV shape resonance can be ruled out through the sequential dissociation channel (6a) as well. This suggests that this channel (both sequential and concerted) is relevant for only the 6–12 eV Feshbach resonances.

Another possibility arises from the $\text{C}_2\text{H}_5\text{O}^-$ fragment. During the C–O dissociation near the keto site, $\text{C}_2\text{H}_5\text{O}^-$ is also a potential fragment [as shown in channel (3a)]. This $\text{C}_2\text{H}_5\text{O}^-$ ion can sequentially dissociate, producing the HCCO^- ions. In this fragmentation process, four C–H bonds can dissociate simultaneously, accompanied by the formation of two H–H bonds. The process can be represented as follows:



As discussed earlier, this dissociation can occur either as a concerted process through structural rearrangements in the TNI or as a sequential dissociation process. The computed threshold for this dissociation channel is 3.85 eV. Consequently, we can exclude channel (6b) for the production of HCCO^- associated with the 3.3 eV resonance.

This observation indicates that, for the 3.3 eV shape resonance, the formation of the HCCO^- ion is not possible when the dissociation occurs near the keto site, producing molecular H_2 as a by-product. Both channels (6a) and (6b) are relevant only to the 6–12 eV Feshbach resonance.

2. C–O dissociation near the ethyl site

In this dissociation channel, water (H_2O) forms as a by-product [34]. This dissociation involves a concerted three-body process through structural rearrangements in the TNI. In this process, two C–H bonds dissociate from the acetate (CH_3COO) site, one C–O bond dissociates, and two O–H bonds form, resulting in the production of H_2O [channel (6c)]. The formation of HCCO^- from the acetate site was observed in previous studies [34,35]. In a recent report on DEA to acetic acid, Chakraborty *et al.* [35] identified a strong signal for the HCCO^- ions around 2 and 10 eV, which exactly matches the structure of HCCO^- ions observed in the present study. The authors attributed the formation of HCCO^- to structural rearrangements in the acetic acid TNI, where H_2O is formed as a by-product. A similar structural rearrangement can occur in the acetate site of the ethyl acetate TNI, resulting in the formation of HCCO^- anions. Therefore, we suggest channel (6c) is the most likely fragmentation channel for the HCCO^- formation. We discard the sequential dissociation process through the formation of the CH_3COO^- due to its extremely stable configuration. The computed threshold energy for this

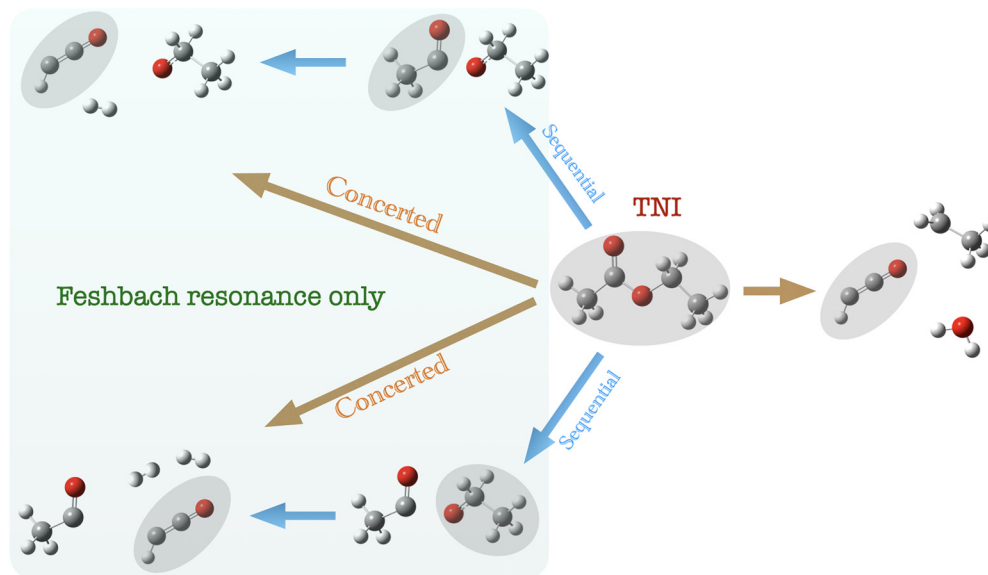


FIG. 7. Suggested fragmentation pathways of ethyl acetate producing HCCO^- during the DEA process. Structural rearrangements in the molecular anion must occur. The two fragmentation channels on the left show the pathways when the C–O dissociation occurs near the keto site of the molecule, whereas the right pathway represents when the C–O dissociation occurs near the ethyl group.

channel is 2.73 eV.



This observation indicates that, for the 3.3 eV shape resonance, this is the sole dissociation channel capable of producing HCCO^- . This dissociation is also highly probable for the 6–12 eV resonance as well.

IV. CONCLUSIONS

The investigation of DEA to ethyl acetate within the 1 to 13 eV energy range using a QMS revealed a shape resonance around 3 eV, accompanied by multiple core-excited Feshbach resonances in the 5 to 12 eV energy region. Fragment anions with six different masses were observed, and the production

of $(M - \text{H})^-$, CH_3^- , CH_3CO^- , $\text{C}_2\text{H}_5\text{O}^-$, and CH_3COO^- ions was justified by single-bond breakage. However, the formation of HCCO^- involved a complex dissociation mechanism. Our experimental findings, combined with theoretical calculations, provide insight into the potential dissociation mechanisms leading to HCCO^- formation. It is suggested that three-body or higher-order dissociations may be involved in all these dissociation channels.

ACKNOWLEDGMENTS

D.C., S.P., and I.C. are supported by the U.S. Department of Energy, Office of Science, Office of Basic Energy Sciences, under Award No. DE-FC02-04ER15533 (NDRL No. 5420) for the work performed at Notre Dame Radiation Laboratory. A.P. deeply appreciates the Council of Scientific and Industrial Research (CSIR) for financial assistance.

-
- [1] E. Illenberger and J. Momigny, *Gaseous Molecular Ions: An Introduction to Elementary Processes Induced by Ionization*, Topics in Physical Chemistry, Vol. 2 (Steinkopff Verlag, Springer-Verlag, Darmstadt, New York, 1992).
- [2] S. Ptasinska, M. T. d. N. Varela, M. A. Khakoo, D. S. Slaughter, and S. Denifl, *Eur. Phys. J. D* **76**, 179 (2022).
- [3] D. Chakraborty and D. Nandi, *Phys. Rev. A* **102**, 052801 (2020).
- [4] O. May, J. Fedor, and M. Allan, *Phys. Rev. A* **80**, 012706 (2009).
- [5] M. Zawadzki, M. Čížek, K. Houfek, R. Čurík, M. Ferus, S. Civiš, J. Kočíšek, and J. Fedor, *Phys. Rev. Lett.* **121**, 143402 (2018).
- [6] D. Chakraborty, L. Eckermann, I. Carmichael, and S. Ptasinska, *J. Chem. Phys.* **153**, 224306 (2020).
- [7] A. Paul, S. Ghosh, and D. Nandi, *Phys. Chem. Chem. Phys.* **25**, 28263 (2023).
- [8] D. Chakraborty, D. S. Slaughter, and S. Ptasinska, *Phys. Rev. A* **108**, 052806 (2023).
- [9] Q. B. Lu and L. Sanche, *Phys. Rev. Lett.* **87**, 078501 (2001).
- [10] B. Boudaiffa, P. Cloutier, D. Hunting, M. A. Huels, and L. Sanche, *Science* **287**, 1658 (2000).
- [11] W. Riemenschneider and H. M. Bolt, Esters, Organic, *Ullmann's Encyclopedia of Industrial Chemistry* (John Wiley & Sons, Ltd, 2005).
- [12] G. V. Buxton, J. Wang, and G. A. Salmon, *Phys. Chem. Chem. Phys.* **3**, 2618 (2001).

- [13] G. Schneider, S. Gohla, J. Schreiber, W. Kaden, U. Schönrock, H. Schmidt-Lewerkühne, A. Kuschel, X. Petsitis, W. Pape, H. Ippen, and W. Diembeck, Skin cosmetics, *Ullmann's Encyclopedia of Industrial Chemistry* (John Wiley & Sons, Ltd, 2001).
- [14] K. Ramalakshmi and B. Raghavan, *Crit. Rev. Food Sci. Nutr.* **39**, 441 (1999).
- [15] W. W. Tan, B. Wu, Y. Wei, and N. Yoshikai, *Org. Synth.* **95**, 1 (2003).
- [16] E. Fischer and A. Speier, *Ber. Dtsch. Chem. Ges.* **28**, 3252 (1895).
- [17] D. C. Forbes and K. J. Weaver, *J. Mol. Catal. A: Chem.* **214**, 129 (2004).
- [18] D. Helmig, J. Müller, and W. Klein, *Chemosphere* **19**, 1399 (1989).
- [19] Y. Pariat and M. Allan, *Int. J. Mass Spectrom. Ion Processes* **103**, 181 (1991).
- [20] L. Feketeová, A. Pelc, A. Ribar, S. E. Huber, and S. Denifl, *Astron. Astrophys.* **617**, A102 (2018).
- [21] C. König, J. Kopyra, I. Bald, and E. Illenberger, *Phys. Rev. Lett.* **97**, 018105 (2006).
- [22] D. Rapp and D. D. Briglia, *J. Chem. Phys.* **43**, 1480 (1965).
- [23] M. J. Frisch *et al.*, GAUSSIAN 16, revision C.01 (Gaussian Inc., Wallingford CT, 2016).
- [24] J. M. L. Martin and G. de Oliveira, *J. Chem. Phys.* **111**, 1843 (1999).
- [25] A. D. Becke, *J. Chem. Phys.* **98**, 5648 (1993).
- [26] T. H. Dunning, *J. Chem. Phys.* **90**, 1007 (1989).
- [27] E. C. Barnes, G. A. Petersson, J. A. J. Montgomery, M. J. Frisch, and J. M. L. Martin, *J. Chem. Theory Comput.* **5**, 2687 (2009).
- [28] S. A. Pshenichnyuk and N. L. Asfandiarov, *Phys. Chem. Chem. Phys.* **22**, 16150 (2020).
- [29] M. A. Śmialek, M. Łabuda, J. Guthmuller, M.-J. Hubin-Franskin, J. Delwiche, S. V. Hoffmann, N. C. Jones, N. J. Mason, and P. Limão-Vieira, *Eur. Phys. J. D* **70**, 138 (2016).
- [30] V. S. Prabhudesai, A. H. Kelkar, D. Nandi, and E. Krishnakumar, *Phys. Rev. Lett.* **95**, 143202 (2005).
- [31] S. Ptasńska, S. Denifl, B. Mróz, M. Probst, V. Grill, E. Illenberger, P. Scheier, and T. Märk, *J. Chem. Phys.* **123**, 124302 (2005).
- [32] D. Chakraborty, P. Nag, and D. Nandi, *Phys. Chem. Chem. Phys.* **18**, 32973 (2016).
- [33] D. Chakraborty and A. Paul, *J. Phys. B* **56**, 142001 (2023).
- [34] W. Sailer, A. Pelc, M. Probst, J. Limtrakul, P. Scheier, E. Illenberger, and T. D. Märk, *Chem. Phys. Lett.* **378**, 250 (2003).
- [35] D. Chakraborty, G. Kharchilava, I. Carmichael, and S. Ptasinska, *J. Phys. B* **56**, 245202 (2023).